

## Article

# Effects of Greening Areas and Water Bodies on Urban Microclimate in Wuhan—A Simulation Study Considering Prospective Planning

Qinli Deng <sup>1</sup>, Zeng Zhou <sup>2,\*</sup>, Xiaofang Shan <sup>1</sup>, Chuancheng Li <sup>1</sup> and Daoru Liu <sup>1,3,\*</sup>

<sup>1</sup> School of Civil Engineering and Architecture, Wuhan University of Technology, Wuhan 430070, China; deng4213@whut.edu.cn (Q.D.); xfshan@whut.edu.cn (X.S.); licc@whut.edu.cn (C.L.)

<sup>2</sup> School of Urban Planning, Wuhan University, Wuhan 430070, China

<sup>3</sup> Department of the Built Environment, Eindhoven University of Technology, P.O. Box 513, 5600 MB Eindhoven, The Netherlands

\* Correspondence: haomaoz@whu.edu.cn (Z.Z.); d.liu@tue.nl (D.L.);  
Tel.: +86-55-2724-7191 (Z.Z.); +31-62-0137-820 (D.L.)

**Abstract:** To alleviate the urban heat island effect and reduce the consumption of electricity and expenditure caused by active cooling devices on hot days, many cities in tropical and subtropical areas emphasize the utilization of urban greening areas in current and future urban planning. We utilized the weather research and forecasting model (WRF) to simulate and study the impact of different greening area rates on the urban microclimate in business, residential, and industrial areas in Wuhan city. Meanwhile, we proposed two efficiency coefficients to evaluate the variable cooling benefit of the improvement of the greening area. The results show that greening areas and water bodies are the cooling sources of cities and that industrial areas benefit the most from improvements in the greening rate, with the average temperature declining by 1.06 °C with a 20% increase in the greening rate, while the corresponding values of residential and industrial areas were 0.98 °C and 0.92 °C, respectively. This research provides a reference for the future planning of tropical and subtropical areas to help improve the urban microclimate, thermal environment, and environmental comfort on hot days.

**Keywords:** heat island effect; urban planning; greening rate; WRF model; hot summer; cold winter region



**Citation:** Deng, Q.; Zhou, Z.; Shan, X.; Li, C.; Liu, D. Effects of Greening Areas and Water Bodies on Urban Microclimate in Wuhan—A Simulation Study Considering Prospective Planning. *Atmosphere* **2022**, *13*, 725. <https://doi.org/10.3390/atmos13050725>

Academic Editors: Sen Chiao, Robert Pasken, Ricardo Sakai, Belay Demoz and Chuan Yao Lin

Received: 18 March 2022

Accepted: 29 April 2022

Published: 2 May 2022

**Publisher's Note:** MDPI stays neutral with regard to jurisdictional claims in published maps and institutional affiliations.



**Copyright:** © 2022 by the authors. Licensee MDPI, Basel, Switzerland. This article is an open access article distributed under the terms and conditions of the Creative Commons Attribution (CC BY) license (<https://creativecommons.org/licenses/by/4.0/>).

## 1. Introduction

Since the 1950s, the temperature increase rate in East Asian megacities such as Tokyo, Shanghai, and Wuhan has been higher than the global average. Factors such as urban extension, the release of anthropogenic heat, and the degradation of green coverage due to urbanization have significantly changed the microclimate of cities and have caused diverse environmental problems [1–7]. The overall result of these variations is the enhanced urban heat island effect (UHIE) in urban areas [3,8–13].

Owing to the additional electricity consumption and burden on the power system caused by UHIE, urban heat islands (UHIs) have been extensively investigated in cities in different areas [14–21]. Some researchers have focused on the influence of urbanization on the urban microclimate and regional meteorological processes [22–24], contributions of urban temperature rising to global warming [25–28], variations in urban precipitation [29–33], and air moisture and water evaporation in cities [34–37]. Meanwhile, the synthetic impact of greening areas and water bodies has largely been ignored due to the complexity and difficulty of considering so many parameters during on-site measurements. Based on these concerns, the weather research and forecasting (WRF) model can be used as a convenient and effective tool to study UHI while considering both the greening areas and water bodies [38–43]. Kitao et al. [44] described the influence of urbanization on UHIs in the Osaka

region considering land use in the past and present using a mesoscale meteorological WRF model. The results showed good compatibility of the measured and simulated data. Hara et al. [45] investigated the increase in the urban island effect intensity (UHII) in the Tokyo metropolitan area caused by global climate change. A high-resolution numerical climate model was utilized to study the present and future UHII in this research. A 20% increase in UHII was found during the night, which was attributed to global warming. The daytime surface air temperature rose more slowly in urban areas than in rural areas because of the better capacity for heat storage in urban regions. Using the regional atmospheric model and pseudo-global warming method, Iizuka et al. [46,47] studied the urban thermal environment during summers in the Nagoya metropolitan area in the 2070s. The results demonstrated that the air temperature in this area would increase more than was expected by the Intergovernmental Panel on Climate Change (IPCC) in the future. Giridharan et al. [48] conducted a six-month investigation including three seasons at seven sites within the coastal area in Hong Kong. A UHII from  $-1.3$  °C to  $3.4$  °C was observed in this study, and a more considerable impact of the season switch than geographical factors on the UHI was identified. Wong et al. [49] studied the UHI at different locations considering multiple parameters within Hong Kong using mathematic analysis. The impacts of air pollution, green space, anthropogenic heat, building density, building height, and air temperature on UHI were compared by correlation analysis to determine the contribution of each factor to the overall UHI. Zhang et al. [50] compared ambient temperature variations in urban areas and irrigated cropland in the Yangtze River Delta to investigate the effect of urbanization on UHI. The results showed that the mean near-surface temperature in urbanized areas increases by  $0.45 \pm 0.43$  °C in winter and by  $1.9 \pm 0.55$  °C in summer. Du et al. [51] took Shanghai City as an example and conducted a multiple-principle analysis to realize the retrieval of remote sensing data in order to study the impacts of construction land, bare land, green land, agricultural land, and water bodies on the urban thermal environment. Construction land was found to contribute most to the local UHI. Using a grid-based model and normalized difference vegetation index (NDVI), Wu et al. [52] analyzed the cooling potential of water bodies and vegetarian cover and discussed the feasibility of urban planning to mitigate UHI. Lin et al. [53] used an innovative mesoscale WRF model coupled with a Noah land surface model and an urban canopy model to study the UHI impact on boundary-layer development and land–sea circulation in northern Taiwan. The robustness of the WRF model and related simulation tools are validated in urban microclimate research. However, the integrated impact of greening areas and water bodies has rarely been discussed in simulations when researchers have talked about future urban planning.

With the deepening of the urbanization process, cities in the hot summer and cold winter (HSCW) area are becoming some of the most developed and densely populated parts of China. These areas possess rich greening and water resources. Urbanization is accompanied by large-scale urban planning and construction, while appropriate planning could effectively limit the increase in urban temperature, alleviate UHIE, and reduce the electricity consumption of refrigeration and active cooling on hot days. A comprehensive investigation considering the local conditions (green/water resources) and future planning would prove to be a useful reference for urban construction. In this study, a numerical simulation in Wuhan City was conducted to classify the impacts of the greening area rate on urban climate for consideration in future urban planning. The results of this study can be utilized to instruct prospective urban planning in cities with similar climatic/environmental conditions to Wuhan City.

## 2. Materials and Methods

### 2.1. Site Selection

The selected area in this study is situated in Wuhan City. The area is a typical example of a region affected by UHI. Wuhan is located at  $113^{\circ}41' - 115^{\circ}05'$  East,  $29^{\circ}58' - 31^{\circ}22'$  North, and it lies to the east of the Jiangnan Plain at the intersection of the middle reaches of

the Yangtze River and Hanjiang River (Figure 1). Over the past four decades, the air temperature has increased by 3 °C at a height of about 1.5 m in Wuhan City due to urbanization and city expansion [54].

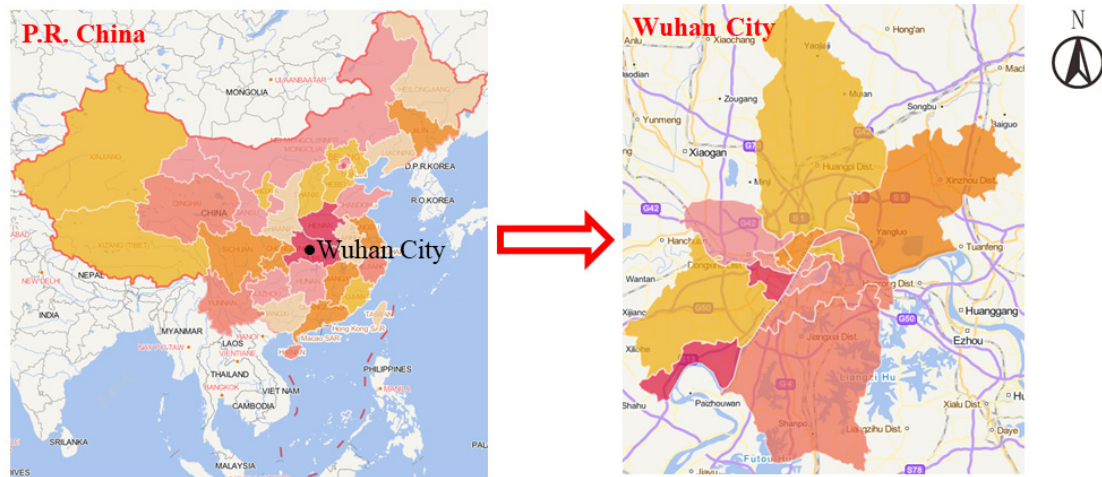


**Figure 1.** Selected research location (<https://en.tianditu.gov.cn/> (accessed on 14 March 2021)).

Wuhan City (30°31" N, 114°18" E, in central China) has a population of more than 10 million and is the biggest city in China by area. The Yangtze River, the longest in China, flows through the city, which experiences a mostly subtropical monsoon climate with hot summers and abundant rainfall. The average annual temperature in Wuhan ranges from 16.5 to 18.5 °C, but temperatures can exceed 40 °C at times (Figure 2) [55].

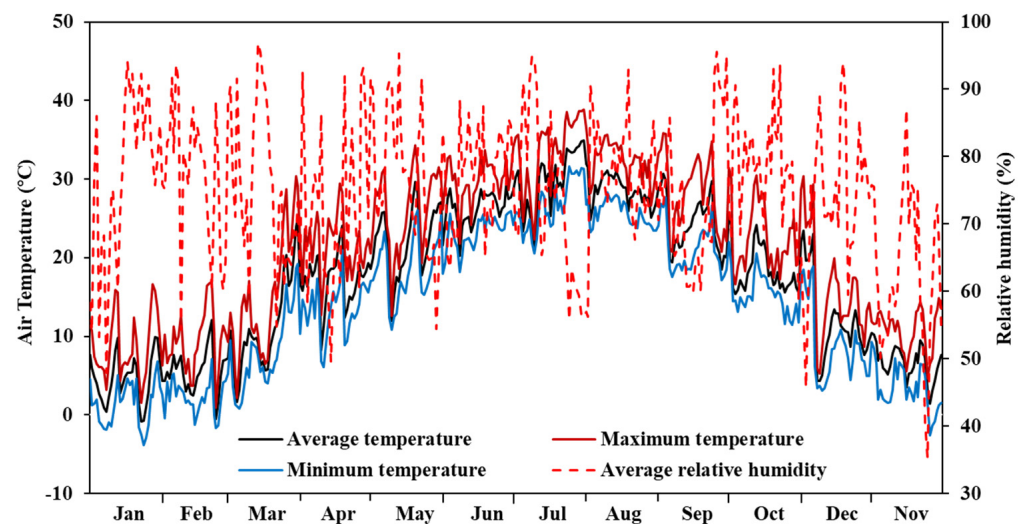


**Figure 2.** Daily temperature and relative humidity in Wuhan.

## 2.2. Numerical Model

In the present study, the Advanced Research WRF dynamical solver, together with other components of the WRF system that are compatible with that solver, was used to produce a simulation. Three-stage nests were configured in the WRF model. Figure 3 shows the domains for the calculation.

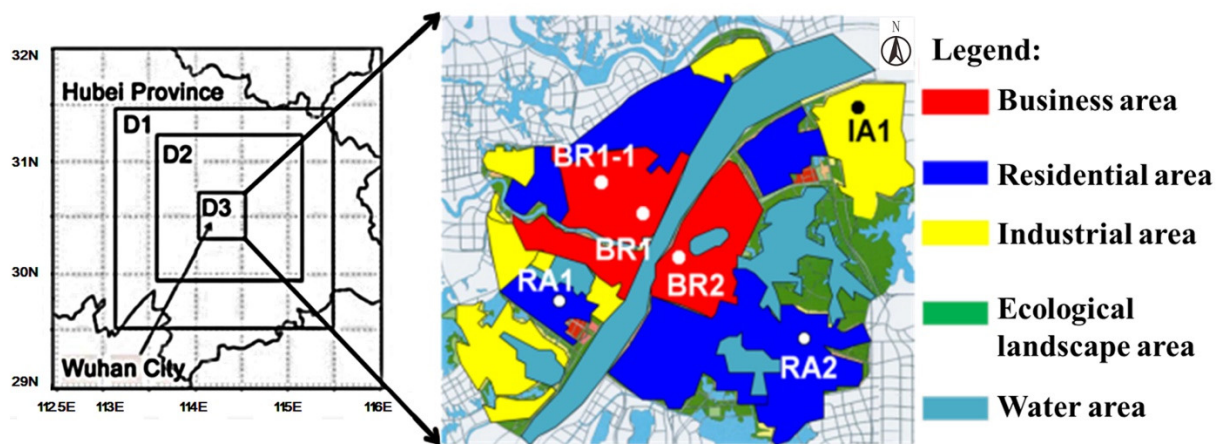


Figure 3. Computational domains and locations.

Domain 3 included the entire area of the built-up zone of Wuhan City centered at 114.30° E, 30.50° N. Further details on the computational domains and grid arrangements are listed in Table 1 [56]. The resolution of the horizontal grid of domain 3 was 0.5 km. The vertical dimension was non-uniform and divided into 35 layers from the ground surface up to an altitude of approximately 20 km. Domain 1 runs downscale along the NCEP reanalysis meteorology field and supplies the initial and lateral boundary conditions for domain 2 every 6 h. Domain 2 is also supplies domain 3 in the same manner.

Table 1. Computational domains and grid arrangements [56].

	Domain X (km) × Y (km)	Grid Number (X × Y × Z)	Grid Size (km)
D1	225 × 225	50 × 50 × 35	4.5
D2	150 × 150	100 × 100 × 35	1.5
D3	50 × 50	100 × 100 × 35	0.5

The parameterization schemes used in our simulation are listed in Table 2 [56]. In this study, we chose a single-layer urban canopy model (UCM) in the WRF model [57,58]. The urban canopy layer is the closest layer to the land surface below the top of the buildings. The WRF/UCM can calculate the following influencing factors: (1) blocking effect of air-flow on buildings and vegetation; (2) turbulence effects around buildings and vegetation; and (3) shading effect of vegetation. These are very important factors when discussing the effect of the green rate on the urban heat island.

From weather data representative of a typical year in Wuhan, the highest temperatures are observed in July, with values above 32 °C from 23 to 31 July. Therefore, the simulation time was set from 08:00 local standard time (LST) on the 21st of July to 08:00 LST on the 1st of August 2020. The model output was generated every hour. National Centers for Environmental Prediction (NCEP) Final Operational Global Analysis data with a horizontal resolution of 1° × 1° in the year 2020 were used to provide the initial and boundary conditions. Twenty-four categories of land use and land cover data provided by the US Geological Survey (USGS) were applied as geographic data in this study.

**Table 2.** WRF configurations.

<b>Time</b>	<b>8:00 am, 21 June 2020 to 8:00 am, 1 August 2020</b>
<b>Meteorological data</b>	Operational global analysis data (National Centers for Environmental Prediction)
<b>Geographic data</b>	US Geological Survey
<b>Long-wave radiation</b>	Rapid and Accurate Radiative Transfer Model (RRTM) longwave radiation scheme
<b>Surface layer</b>	Monin Obukhov scheme
<b>Land surface</b>	Noah land surface model and Single layer urban canopy model (UCM)
<b>Cumulus</b>	Kain–Fritsch (new Eta) scheme
<b>Short-wave radiation</b>	Dudhia scheme
<b>Micro-physics</b>	WRF Single-Moment 6-class
<b>Boundary layer</b>	Yonsei University (YSU) PBL

### 2.3. Case Design

As shown in Figure 4, Wuhan City is divided into three zones: the business area (Zone 1), the residential area (Zone 2), and the industrial area (Zone 3). According to the comprehensive planning of Wuhan City from 2020 to 2030, five cases were designed (Table 3). From case 1 to case 5, the building density is 40% in Zone 1, 35% in Zone 2, 30% in Zone 3; the greening area rate is increased gradually from 20% to 40% in Zone 1, from 25% to 45% in Zone 2, and from 30% to 50% in Zone 3. The land utilization types in the three zones are as follows: building, greening, and roads.

**Table 3.** Parameters of case design.

<b>Variables</b>		<b>Case 1</b>	<b>Case 2</b>	<b>Case 3</b>	<b>Case 4</b>	<b>Case 5</b>
<b>Building density (%)</b>	<b>Zone1</b>	40	40	40	40	40
	<b>Zone2</b>	35	35	35	35	35
	<b>Zone3</b>	30	30	30	30	30
<b>Greening rate (%)</b>	<b>Zone1</b>	20	25	30	35	40
	<b>Zone2</b>	25	30	35	40	45
	<b>Zone3</b>	30	35	40	45	50
<b>Roof_width (m)</b>	<b>Zone1</b>	45	45	45	45	45
	<b>Zone2</b>	40	40	40	40	40
	<b>Zone3</b>	35	35	35	35	35
<b>Road_width (m)</b>	<b>Zone1</b>	10	10	10	10	10
	<b>Zone2</b>	10	10	10	10	10
	<b>Zone3</b>	10	10	10	10	10
<b>Frc_urb (fraction)</b>	<b>Zone1</b>	0.8	0.75	0.7	0.65	0.6
	<b>Zone2</b>	0.75	0.7	0.65	0.6	0.55
	<b>Zone3</b>	0.7	0.65	0.6	0.55	0.5

In this paper, we compare the data at five points as shown in Figure 3 (Zone 1: BR1, BR2; Zone 2: RA1, RA2; Zone 3: IA1).

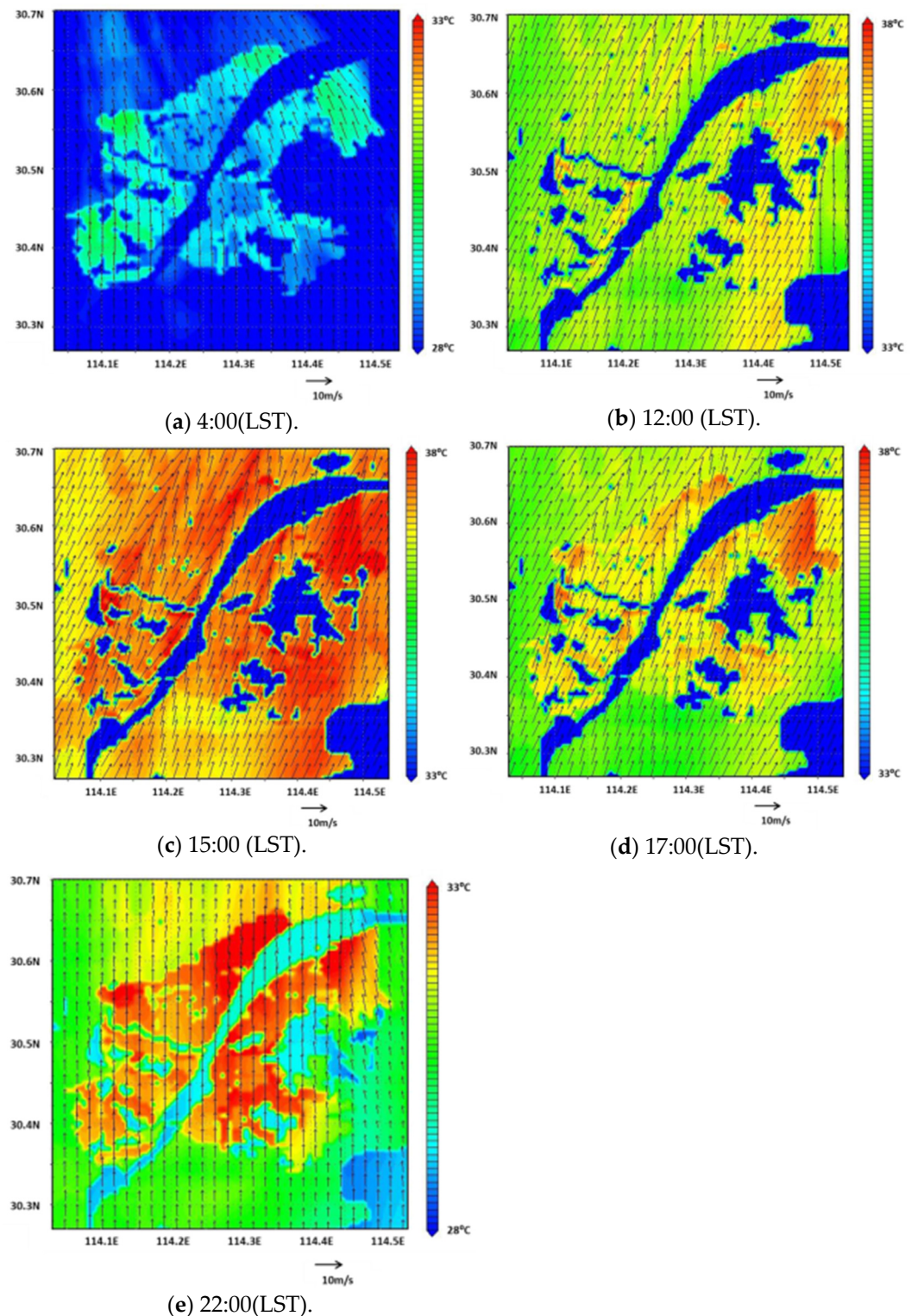


**Figure 4.** Air temperature and wind velocity of domain 3 on 31 July.

#### 2.4. Efficiency of Cooling Effect of Greening Area

Generally, greening area and green land are considered to have the capacity to cool adjacent areas in hot seasons. This capacity is called the cooling effect of the greening area/land (CEGA) [59–61]. In previous studies, CEGA has been widely and deeply researched using various methods, including on-site investigations, numerical simulations, and remote sensing. However, research on the efficiency of this effect and methods to

estimate its efficiency is limited. In this study, we propose a difference coefficient to identify the change in cooling efficiency when the greening area rate is changed ( $E_{cc}$ ).

$$E_{cc.s_2-s_1} = \frac{1}{C_{s_2} - C_{s_1}}(T_{s_1} - T_{s_2}) \tag{1}$$

where  $C_{s_i}$  is the greening area rate of each area,  $T_{s_i}$  is the average air temperature at the corresponding greening rate ( $i = 1,2$ ), and  $E_{cc.s_2-s_1}$  represents the cooling efficiency when the cooling area rate of each area changes from  $C_{s_1}$  to  $C_{s_2}$ . The higher the value of  $E_{cc}$ , the better the benefit of cooling brought about by increasing the greening rate. For realistic comparisons, we kept the difference in the greening rate at 20%; that is,  $C_{s_2} - C_{s_1} = 20\%$ .

### 3. Results and Discussion

#### 3.1. Overall Regional Temperature Distribution

Figure 4 shows the air temperature at a 2 m height in domain 3 at 4:00 (LST), 12:00 (LST), 15:00 (LST), 17:00 (LST), and 22:00 (LST) on 31 July in Case 3 (2020). The maximum temperature in this section was clearly observed at 15:00. The hottest region was found in the industrial zone (IA1), where the maximum air temperature exceeded 37 °C. Meanwhile, there are always low-temperature circles at the edges of the water bodies in Figure 5. This means that regions surrounded by water bodies were colder than other areas, and then the water body inside the urban area acted as a cold source for the entire region.

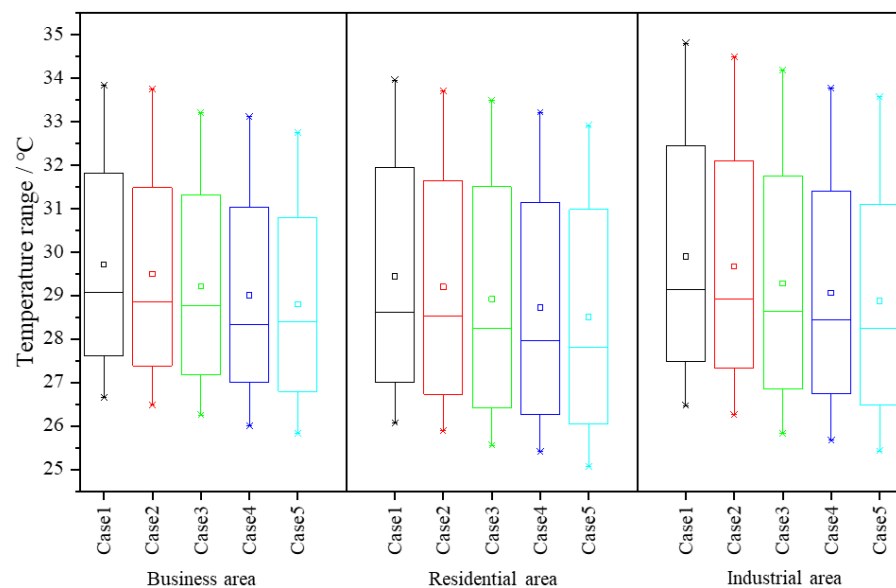


**Figure 5.** Daily temperature variation of five cases in the business, residential, and industrial areas.

#### 3.2. Impact of Greening Area on the Regional Air Temperature

Figure 5 shows the distribution of air temperature in three kinds of areas under various greening area rates. In general, regional air temperature decreases with an increase in the greening area rate. The daily average air temperature in the industrial area is the highest, followed by the business area, and the average daily temperature in the residential area is the lowest. The range of daily temperature change in the business area is small, while that in the residential and industrial areas is relatively large. At the same time, the changing intensity of the cooling effect is different at different times of the day.

Figure 6 shows the daily air temperature variation of five cases in the business area, residential area, and industrial area. In each zone, air temperature decreases with an increase in greening area rate at all times. However, the impact of the green rate on air temperature is different at different times of the day.

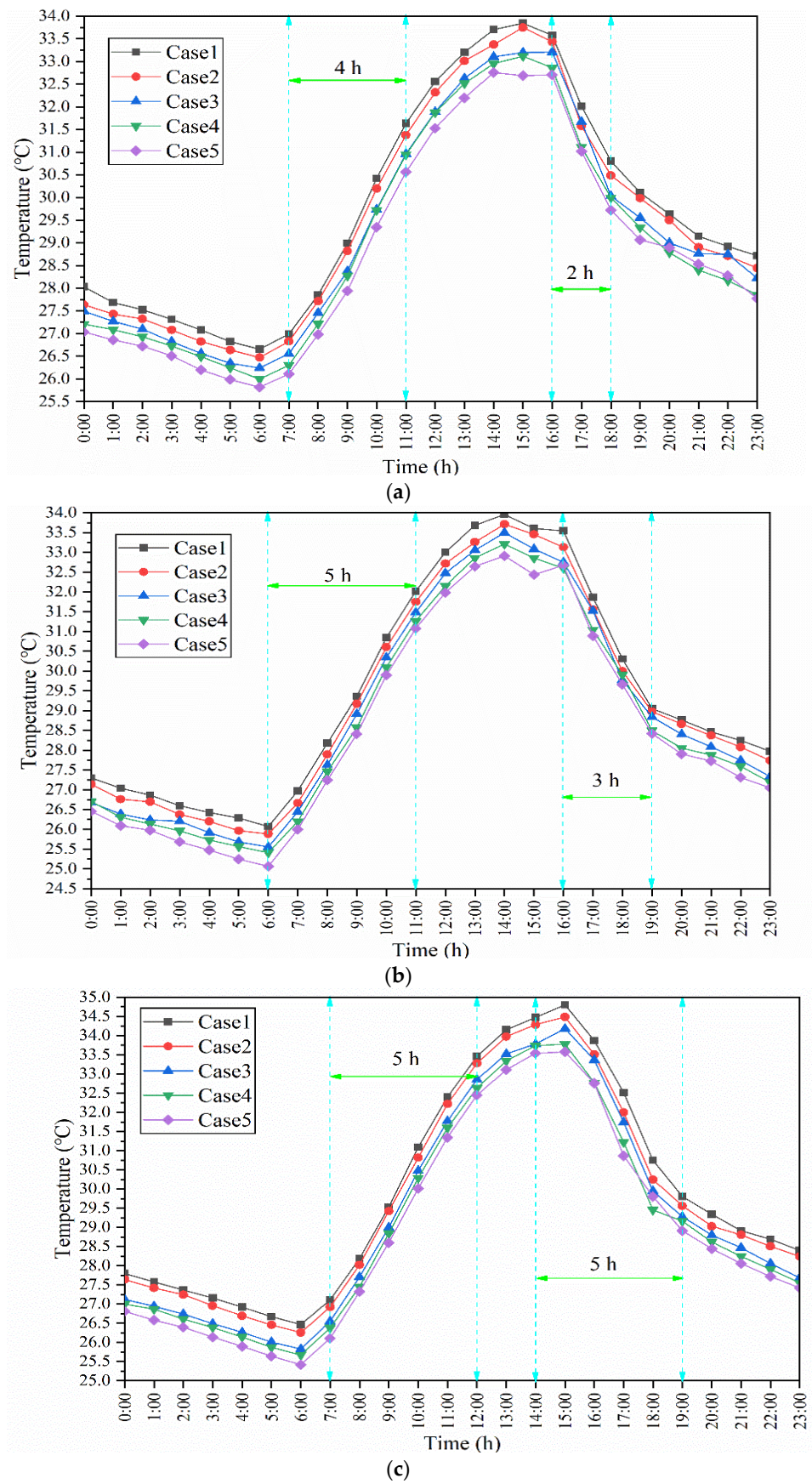


Figure 6. Daily air temperature variation in the (a) business, (b) residential, and (c) industrial areas.

In the business area, the daily minimum temperature occurs at 6:00 and the daily maximum temperature occurs at 15:00. During 0:00–7:00, the CEGA is steady, while every 5% increment in the greening area rate brings a temperature decline of about 0.25 °C. During 7:00–11:00 and 16:00–18:00, the cooling effect of the greening area is limited. During 11:00–16:00 and 18:00–23:00, the cooling effect of the greening area is relatively complex. The duration of 9:00–13:00 is a special duration; the air temperatures of Case 3 (30% of green rate) and Case 4 (35% of green rate) are almost the same at that time.

In the residential area, the daily minimum temperature occurs at 6:00 and the daily maximum temperature occurs at 14:00. During 0:00–6:00, the cooling effect of the greening area is relatively steady, with slight destabilization. During 6:00–11:00, every 5% increment in the greening area rate brings a temperature decline slightly over 0.25 °C. During 14:00–16:00, the cooling effect of the greening area is enhanced. During 16:00–19:00 and 18:00–23:00, the cooling effect of the greening area is relatively complex and disordered. After 19:00, the impact of the greening area on air temperature changes to the same condition as 0:00–6:00.

In the industrial area, the daily minimum temperature occurs at 6:00 and the daily maximum temperature occurs at 15:00. During 0:00–7:00, the CEGA is steady; however, the decline in air temperature is nonlinear with the increase in the greening area rate. During 7:00–12:00, CEGA is limited and steady, while every 5% increment in the greening area rate brings a temperature decline slightly below 0.25 °C. During 14:00–19:00, the CEGA is complex with irregular destabilization. The impact of the greening area at 19:00–23:00 is similar to that at 0:00–7:00.

Considering the actual situation of the diurnal variation in the hot season in Wuhan City, and combining the analysis from Figure 6, we selected four time nodes in a day in each area to analyze the change in the benefit from the greening area. Table 4 compares the  $E_{cc}$  of different areas at 4:00, 10:00, 16:00, and 22:00.

**Table 4.**  $E_{cc}$  of four times in different areas.

Variables	Time	$C_{s2}$	$C_{s1}$	$T_{s1}$	$T_{s2}$	$E_{cc.s2-s1}$
	h	%	%	°C	°C	°C
Business	04:00	40	20	27.08	26.20	4.42
	10:00	40	20	30.42	29.35	5.36
	16:00	40	20	33.58	32.71	5.13
	22:00	40	20	29.02	28.08	4.71
Residential	04:00	45	25	26.43	25.48	4.76
	10:00	45	25	30.85	29.90	4.74
	16:00	45	25	33.54	32.67	4.36
	22:00	45	25	28.25	27.31	4.69
Industrial	04:00	50	30	26.92	25.90	5.48
	10:00	50	30	31.09	30.02	5.37
	16:00	50	30	33.87	32.76	5.53
	22:00	50	30	28.69	27.72	4.86

As shown in Table 4, the cooling benefit from the greening area is different in different areas at different times, and the descending order is industrial area, business area, and residential area. In the business area, the cooling benefit from the greening area during the daytime is better than that at nighttime. In the residential area, the cooling effect of the greening area is relatively steady all day, with a slight decline at 16:00–19:00. For the industrial area, the cooling effect and the benefit of the greening area are obvious and largest, and a 20% improvement in the greening rate decreases the average temperature by 1.06 °C.

### 3.3. Impact of Greening Area Rate on the Regional Wind Velocity

Figure 7 shows the daily wind velocity range of the five cases in the business, residential, and industrial areas at a height of 10 m. The average wind speed in the industrial area is the highest, followed by that in the residential area, and the average wind speed in the business area is the lowest. The effect of greening rate change on wind speed is not obvious. For the business area, the fluctuation range of daily wind speed is the largest when the greening rate is 40%, and the fluctuation range of daily wind speed is the smallest when the greening rate is 35%. For the residential area, the fluctuation range of daily wind speed is the largest when the greening rate is 35%, and the fluctuation range of daily wind speed is the smallest when the greening rate is 35%. For the industrial area, the fluctuation range of daily wind speed is the largest when the greening rate is 35%, and the fluctuation range of daily wind speed is the smallest when the greening rate is 20%.

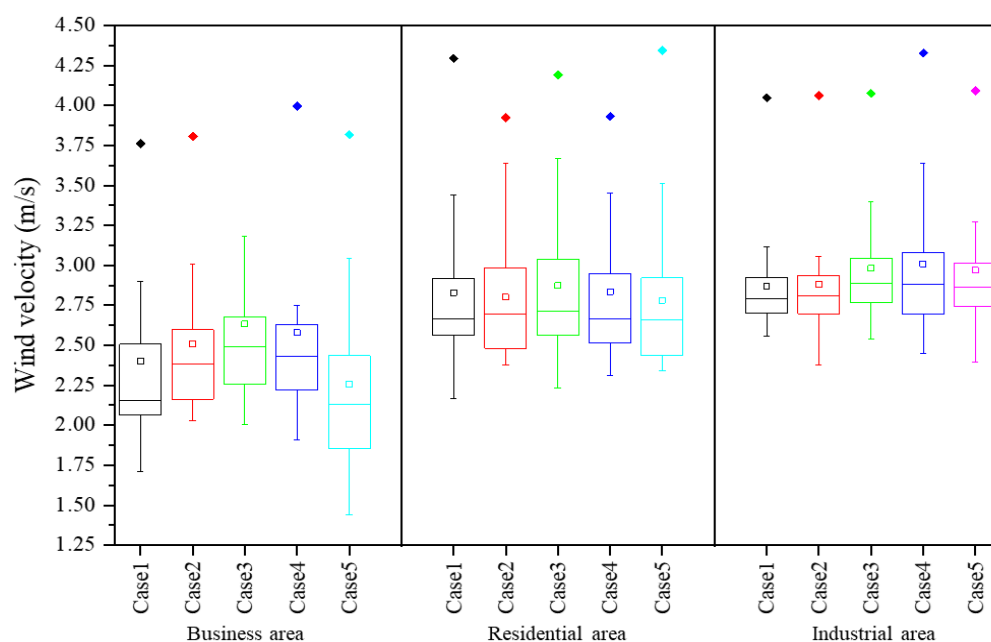


**Figure 7.** Daily variation in wind velocity of five cases in the business, residential, and industrial areas.

Figure 8 shows the wind velocity in different areas at a height of 10 m. In the business area, the impact of the different greening rates on regional wind velocity is complex. The minimum wind velocity is about 1.3 m/s at 22:00 when the greening rate is 40%, and the maximum wind velocity is about 4.6 m/s at 17:00 when the greening rate is 30%. At 9:00–14:00, the impact of the greening area on wind velocity is clearly limited.

In the residential area, the greening area has a limited impact on regional wind velocity. The minimum wind velocity is about 2.1 m/s at 0:00 when the greening rate is 20%, and the maximum wind velocity is about 4.3 m/s at 17:00 when the greening rate is 40%. At the duration of 0:00–15:00, greening land has little impact on regional wind velocity.

In the industrial area, the fluctuation range of wind velocity is larger than that of the residential area but smaller than that of the business area. After 11:00, the wind velocity increases rapidly and falls rapidly after reaching its peak at 14:00, and it reaches its valley at 22:00, with the maximum value being about 4.1 m/s and the minimum value being about 1.3 m/s.

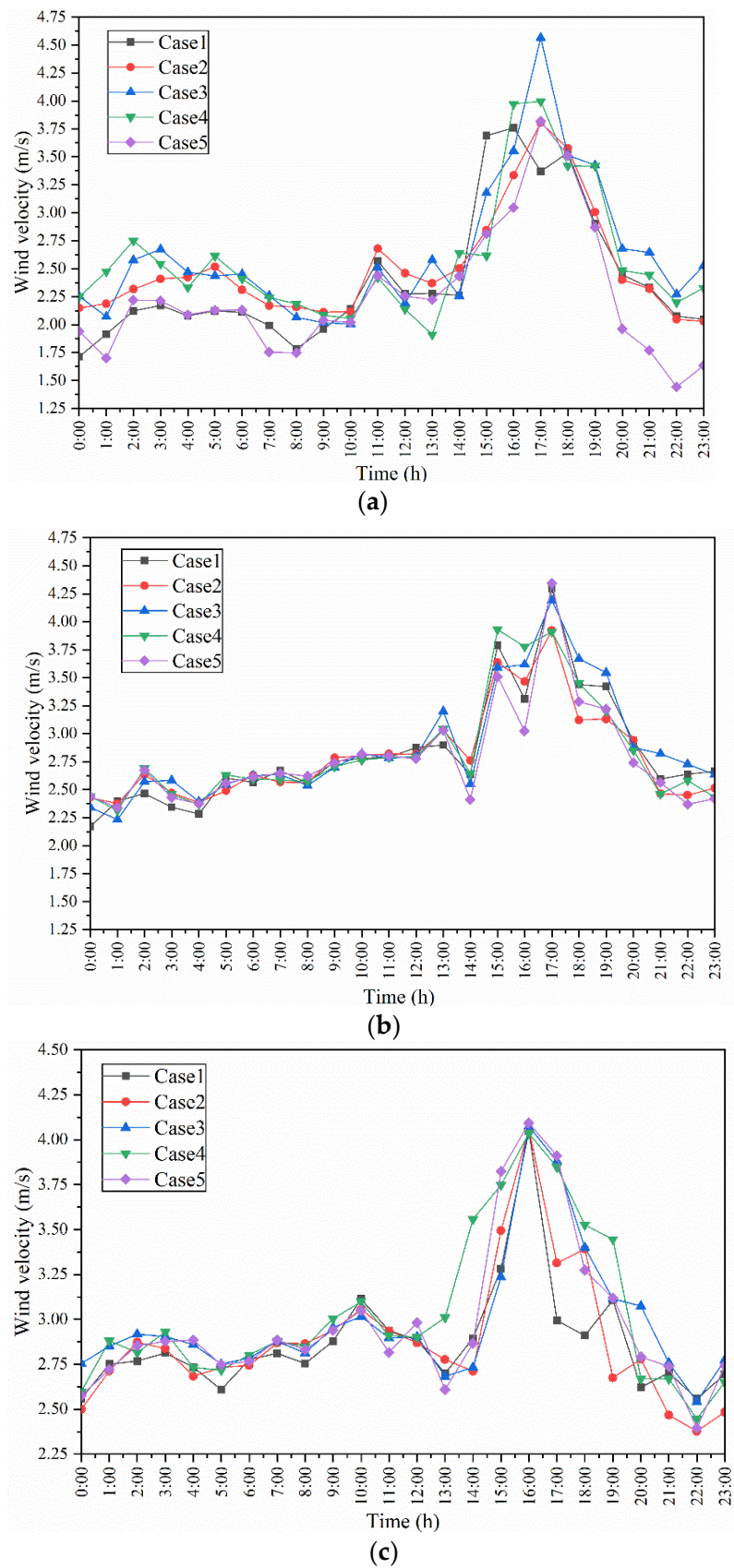


Figure 8. Daily wind velocity variation in the (a) business, (b) residential, and (c) industrial areas.

### 3.4. Limitations of this Study

There are some limitations to this study. Theoretically, the urban microclimate is a multifactor system that is not only affected by greening areas and water bodies, and the exact contribution of these factors to microclimate change has not been established. Secondly, the distribution of greening areas and water bodies is at the horizontal profile, while the vertical geometry of cities (building façade, height, and agglomeration) has a considerable impact on the evolution of the urban microclimate. In addition, in the UCM model used in this study, the anthropogenic heat is not considered due to its large statistics and different regions.

## 4. Conclusions

In this study, the effect of greening areas on urban climate was examined in Wuhan City for the purposes of prospective urban planning. The following conclusions can be drawn:

- (1) Greening areas and water bodies both have the capacity to cool adjacent areas in hot seasons. The cooling effect of greening areas varies in different areas and at different times.
- (2) The industrial areas benefitted the most from the improvement in the greening rate. The average temperature in the area can be reduced by 1.06 °C with a 20% increase in the greening rate. In the business area, the cooling benefit of a 20% increase in the greening rate increase was 0.98 °C, while that of the residential area was 0.92 °C.
- (3) The impact of greening areas and greening rate on regional wind speed is not obvious.

**Author Contributions:** Conceptualization, Q.D.; data curation, Q.D., Z.Z. and X.S.; formal analysis, Q.D. and D.L.; funding acquisition, Q.D. and Z.Z.; methodology, Q.D. and C.L.; resources, Q.D.; software, Q.D.; supervision, Q.D.; writing—original draft, D.L. and Q.D.; writing—review and editing, Q.D. All authors have read and agreed to the published version of the manuscript.

**Funding:** This project was funded by the National Natural Science Foundation of China (51608405; 51808410).

**Institutional Review Board Statement:** Not applicable.

**Informed Consent Statement:** Not applicable.

**Data Availability Statement:** Not applicable.

**Conflicts of Interest:** The authors declare no conflict of interest.

## References

1. Kimura, F.; Takahashi, S. The effects of land-use and anthropogenic heating on the surface temperature in the Tokyo Metropolitan area: A numerical experiment. *Atmos. Environ. Urban Atmos.* **1991**, *25*, 155–164. [\[CrossRef\]](#)
2. Ohashi, Y.; Genchi, Y.; Kondo, H.; Kikegawa, Y.; Hirano, Y. Influence of Air-Conditioning Waste Heat on Air Temperature in Tokyo during Summer: Numerical Experiments Using an Urban Canopy Model Coupled with a Building Energy Model. *J. Appl. Meteorol. Climatol.* **2007**, *46*, 66–81. [\[CrossRef\]](#)
3. Santamouris, M. Cooling the cities—A review of reflective and green roof mitigation technologies to fight heat island and improve comfort in urban environments. *Sol. Energy* **2014**, *103*, 682–703. [\[CrossRef\]](#)
4. Lee, T.; Meene, S.V.D. Comparative studies of urban climate co-benefits in Asian cities: An analysis of relationships between CO<sub>2</sub> emissions and environmental indicators. *J. Clean. Prod.* **2013**, *58*, 15–24. [\[CrossRef\]](#)
5. Yang, B.; Qian, Y. Simulation of urban climate with high-resolution WRF model: A case study in Nanjing, China. *Asia-Pac. J. Atmos. Sci.* **2012**, *48*, 227–241. [\[CrossRef\]](#)
6. Ma, H.; Jiang, Z.; Jie, S.; Dai, A.; Yang, X.; Fei, H. Effects of urban land-use change in East China on the East Asian summer monsoon based on the CAM5.1 model. *Clim. Dyn.* **2015**, *46*, 1–13. [\[CrossRef\]](#)
7. Narumi, D.; Kondo, A.; Shimoda, Y. Effects of anthropogenic heat release upon the urban climate in a Japanese megacity. *Environ. Res.* **2009**, *109*, 421–431. [\[CrossRef\]](#)
8. Oke, T.R. City size and the urban heat island. *Atmos. Environ.* **2017**, *7*, 769–779. [\[CrossRef\]](#)
9. Kim, H.H. Urban heat island. *Int. J. Remote Sens.* **1991**, *13*, 2319–2336. [\[CrossRef\]](#)
10. Arnfield, A.J. Two decades of urban climate research: A review of turbulence, exchanges of energy and water, and the urban heat island. *Int. J. Climatol.* **2003**, *23*, 1–26. [\[CrossRef\]](#)

11. Oke, T.R. The energetic basis of the urban heat island. *Q. J. R. Meteorol. Soc.* **2010**, *108*, 1–24. [[CrossRef](#)]
12. Memon, R.A.; Leung, D.Y.C.; Liu, C. A review on the generation, determination and mitigation of Urban Heat Island. *J. Environ. Sci.* **2008**, *20*, 120–128.
13. Oke, T.R. Canyon geometry and the nocturnal urban heat island: Comparison of scale model and field observations. *Int. J. Climatol.* **2010**, *1*, 237–254. [[CrossRef](#)]
14. Kim, Y.H.; Baik, J.J. Daily maximum urban heat island intensity in large cities of Korea. *Theor. Appl. Climatol.* **2004**, *79*, 151–164. [[CrossRef](#)]
15. Oke, T.R. Street design and urban canopy layer climate. *Energy Build.* **1988**, *11*, 103–113. [[CrossRef](#)]
16. Unger, J. Intra-urban relationship between surface geometry and urban heat island: Review and new approach. *Clim. Res.* **2004**, *27*, 253–264. [[CrossRef](#)]
17. Kolokotroni, M.; Giridharan, R. Urban heat island intensity in London: An investigation of the impact of physical characteristics on changes in outdoor air temperature during summer. *Sol. Energy* **2008**, *82*, 986–998. [[CrossRef](#)]
18. Memon, R.A.; Leung, D.Y.C.; Liu, C.H. An investigation of urban heat island intensity (UHII) as an indicator of urban heating. *Atmos. Res.* **2009**, *94*, 491–500. [[CrossRef](#)]
19. Khaikine, M.N.; Kuznetsova, I.N.; Kadygrov, E.N.; Miller, E.A. Investigation of temporal-spatial parameters of an urban heat island on the basis of passive microwave remote sensing. *Theor. Appl. Climatol.* **2006**, *84*, 161–169. [[CrossRef](#)]
20. Zhangbao, H.U.; Bingfeng, Y.U.; Chen, Z.; Tiantian, L.L.; Liu, M. Numerical investigation on the urban heat island in an entire city with an urban porous media model. *Atmos. Environ.* **2012**, *47*, 509–518.
21. Emmanuel, R. Summertime Urban Heat Island Mitigation: Propositions based on an Investigation of Intra-Urban Air Temperature Variations. *Archit. Sci. Rev.* **1997**, *40*, 155–164. [[CrossRef](#)]
22. Jin, M.; Dickinson, R.E.; Zhang, D.L. The Footprint of Urban Areas on Global Climate as Characterized by MODIS. *J. Clim.* **2004**, *18*, 1551–1565. [[CrossRef](#)]
23. Ya, M.A.; Kuang, Y.; Huang, N. Coupling urbanization analyses for studying urban thermal environment and its interplay with biophysical parameters based on TM/ETM+ imagery. *Int. J. Appl. Earth Obs. Geoinf.* **2010**, *12*, 110–118.
24. Ren, C.Y.; Wu, D.T.; Dong, S.C. The influence of urbanization on the urban climate environment in Northwest China. *Geogr. Res.* **2006**, *25*, 233–241.
25. Fernando, H.J.S.; Dimitrova, R.; Sentic, S. Climate Change Meets Urban Environment. *Nato Sci. Peace Secur.* **2012**, *125*, 115–133.
26. Lorenz, D.J.; Deweaver, E.T. The Response of the Extratropical Hydrological Cycle to Global Warming. *J. Clim.* **2007**, *20*, 3470–3484. [[CrossRef](#)]
27. Song, U.R.; Saeromi, M.; Changhoi, H.; Eunju, L. Responses of two invasive plants under various microclimate conditions in the Seoul Metropolitan Region. *Environ. Manag.* **2012**, *49*, 1238–1246. [[CrossRef](#)] [[PubMed](#)]
28. Slini, T.; Pavlidou, F.N. Assessing air quality in the urban environment: The gender gap. In *Energy, Transportation and Global Warming*; Springer: Cham, Switzerland, 2016.
29. Schroder, L.J.; Hedley, A.G. Variation in precipitation quality during a 40-hour snowstorm in an Urban Environment—Denver, Colorado. *Int. J. Environ. Stud.* **1986**, *28*, 131–138. [[CrossRef](#)]
30. Olszowski, T.; Ziemcik, Z. An alternative conception of PM 10 concentration changes after short-term precipitation in urban environment. *J. Aerosol Sci.* **2018**, *121*, 21–30. [[CrossRef](#)]
31. Chen, W.D.; Dan-Hong, F.U.; Miao, S.G.; Zhang, Y.Z. Numerical simulation of urban environment impacts on clouds and precipitation in Beijing. *Prog. Geophys.* **2015**, *30*, 983–995.
32. Wang, X.Q.; Wang, Z.F.; Qi, Y.B.; Hu, G. Effect of urbanization on the winter precipitation distribution in Beijing area. *Sci. China* **2009**, *52*, 250–256. [[CrossRef](#)]
33. Wang, J.; Feng, J.; Yan, Z. Potential sensitivity of warm season precipitation to urbanization extents: Modeling study in Beijing-Tianjin-Hebei urban agglomeration in China. *J. Geophys. Res. Atmos.* **2015**, *120*, 9408–9425. [[CrossRef](#)]
34. Adebayo, Y.R. “Heat island” in a humid tropical city and its relationship with potential evaporation. *Theor. Appl. Climatol.* **1991**, *43*, 137–147. [[CrossRef](#)]
35. Liu, J.; Ma, F.; Li, Y. The Impact of Vegetation on Mitigating Heat Island Intensity in Four Major Cities in China. *Adv. Mater. Res.* **2011**, *250–253*, 2935–2938. [[CrossRef](#)]
36. Liu, J.; Ma, F.; Li, F. Analysis of Heat Island Intensity in Urban Blocks Using Coupled Simulation. *Appl. Mech. Mater.* **2011**, *71–78*, 1669–1672. [[CrossRef](#)]
37. Cregg, B.M.; Dix, M.E. Tree moisture stress and insect damage in urban areas in relation to heat island effects. *J. Arboric.* **2001**, *27*, 8–17.
38. Chen, F.; Yang, X.; Zhu, W. WRF simulations of urban heat island under hot-weather synoptic conditions: The case study of Hangzhou City, China. *Atmos. Res.* **2014**, *138*, 364–377. [[CrossRef](#)]
39. Giannaros, T.M.; Melas, D.; Daglis, I.A.; Keramitsoglou, I.; Kourtidis, K. Numerical study of the urban heat island over Athens (Greece) with the WRF model. *Atmos. Environ.* **2013**, *73*, 103–111. [[CrossRef](#)]
40. Meng, W.; Zhang, Y.; Li, J.; Lin, W.; Dai, G.; Li, R. Application of WRF/UCM in the simulation of a heat wave event and urban heat island around Guangzhou. *J. Trop. Meteorol.* **2011**, *17*, 257–267.

41. Shrestha, K.L.; Kondo, A.; Maeda, C.; Kaga, A.; Inoue, Y. Investigating the Contribution of Urban Canopy Model and Anthropogenic Heat Emission to Urban Heat Island Effect using WRF Model. *Trans. Jpn. Soc. Refrig. Air Cond. Eng.* **2011**, *26*, 45–55.
42. Li, H.; Wolter, M.; Xun, W.; Sodoudi, S. Impact of land cover data on the simulation of urban heat island for Berlin using WRF coupled with bulk approach of Noah-LSM. *Theor. Appl. Climatol.* **2017**, *134*, 1–15. [[CrossRef](#)]
43. Bhati, S.; Mohan, M. WRF model evaluation for the urban heat island assessment under varying land use/land cover and reference site conditions. *Theor. Appl. Climatol.* **2016**, *126*, 385–400. [[CrossRef](#)]
44. Kitao, N.; Moriyama, M.; Tanaka, T.; Takebayashi, H. Analysis of Urban Heat Island Phenomenon in Osaka Region Using WRF Model. *J. Environ. Eng.* **2010**, *75*, 465–471. [[CrossRef](#)]
45. Hara, M.; Kusaka, H.; Kimura, F.; Wakazuki, Y. Effect of global climate change on urban heat island intensity of Tokyo metropolitan area-winter season case. *Nagare* **2010**, *29*, 353–361.
46. Iizuka, S.; Kinbara, K.; Kusaka, H.; Hara, M.; Akimoto, Y. A Numerical Simulation of Current Status of Summer and an Attempt to Project a Future Thermal Environment Combined with Pseudo Global Warming Data. *J. Environ. Eng. Trans. AIJ* **2010**, *75*, 87–93. [[CrossRef](#)]
47. Iizuka, S.; Kinbara, K.; Kusaka, H. A long-term projection of a thermal environment in summer of the 2070s, Numerical study on thermal environment in the Nagoya metropolitan area by using WRF (Part 2). *J. Environ. Eng. Trans. AIJ* **2011**, *76*, 425–430. [[CrossRef](#)]
48. Giridharan, R.; Lau, S.S.Y.; Ganesan, S.; Givoni, B. Urban design factors influencing heat island intensity in high-rise high-density environments of Hong Kong. *Build. Environ.* **2007**, *42*, 3669–3684. [[CrossRef](#)]
49. Man, S.W.; Nichol, J.; Kwok, K.H. The urban heat island in Hong Kong: Causative factors and scenario analysis. In *Urban Remote Sensing Event*; Institute of Electrical and Electronics Engineers: New York, NY, USA, 2009.
50. Zhang, N.; Gao, Z.; Wang, X.; Chen, Y. Modeling the impact of urbanization on the local and regional climate in Yangtze River Delta, China. *Theor. Appl. Climatol.* **2010**, *102*, 331–342. [[CrossRef](#)]
51. Du, H.; Ai, J.; Cai, Y.; Jiang, H.; Liu, P. Combined Effects of the Surface Urban Heat Island with Landscape Composition and Configuration Based on Remote Sensing: A Case Study of Shanghai, China. *Sustainability* **2019**, *11*, 2890. [[CrossRef](#)]
52. Wu, Z.; Zhang, Y. Water Bodies' Cooling Effects on Urban Land Daytime Surface Temperature: Ecosystem Service Reducing Heat Island Effect. *Sustainability* **2019**, *11*, 787. [[CrossRef](#)]
53. Lin, C.Y.; Chen, F.; Huang, J.C.; Chen, W.C.; Liou, Y.A.; Chen, W.N.; Liu, S.C. Urban heat island effect and its impact on boundary layer development and land–sea circulation over northern Taiwan. *Atmos. Environ.* **2008**, *42*, 5635–5649. [[CrossRef](#)]
54. Chen, Z.; Wang, H.; Ren, G. Asymmetrical Change of Urban Heat Island Intensity in Wuhan, China. *Adv. Clim. Change Res.* **2007**, *3*, 282–286.
55. Nation Meteorological Information Center. *China's Special Meteorological Data Set for Thermal Environment Analysis*; China Architecture & Building Press: Beijing, China, 2005.
56. Deng, Q.; Zhou, Z.; Li, C.; Mochida, A. Impact of Greening Area Ratio on Urban Climate in Hot-summer and Cold-winter City. In *Proceedings of the 9th International Conference on Urban Climate (ICUC9)*, Toulouse, France, 20–24 July 2015.
57. Kusaka, H.; Kimura, F. Coupling a Single-Layer Urban Canopy Model with a Simple Atmospheric Model: Impact on Urban Heat Island Simulation for an Idealized Case. *J. Meteorol. Soc. Jpn.* **2004**, *82*, 67–80. [[CrossRef](#)]
58. Kusaka, H.; Kondo, H.; Kikegawa, Y.; Kimura, F. A Simple Single-Layer Urban Canopy Model for Atmospheric Models: Comparison With Multi-Layer Additionally, Slab Models. *Bound. -Layer Meteorol.* **2001**, *101*, 329–358. [[CrossRef](#)]
59. Hamada, S.; Tanaka, T.; Ohta, T. Impacts of land use and topography on the cooling effect of green areas on surrounding urban areas. *Urban For. Urban Green.* **2013**, *12*, 426–434. [[CrossRef](#)]
60. Oliveira, S.; Andrade, H.; Vaz, T. The cooling effect of green spaces as a contribution to the mitigation of urban heat: A case study in Lisbon. *Build. Environ.* **2011**, *46*, 2186–2194. [[CrossRef](#)]
61. Kong, F.; Yin, H.; James, P.; Hutyra, L.R.; He, H.S. Effects of spatial pattern of greenspace on urban cooling in a large metropolitan area of eastern China. *Landsc. Urban Plan.* **2014**, *128*, 35–47. [[CrossRef](#)]